Thermal Weakening, Convergent Flow, and Vertical Heat Transport in the Northeast Greenland Ice Stream Shear Margins

N. Holschuh*[1], D. Lilien[1], K. Christianson[1]

[1]Department of Earth and Space Sciences, University of Washington, Johnson Hall Rm-070, Box 351310, 4000 15th Avenue NE, Seattle, Washington 98195-1310

[*]Corresponding author: Nicholas Holschuh (holschuh@uw.edu)

Key Points:

- Thermal weakening is present in the Northeast Greenland Ice Stream (NEGIS) shear margins, despite low strain rates.
- Vertical advection of heat dominates the shear margin temperature structure here, validated by radar reflectivity and isochron geometry.
- Radar data can be used to constrain ice temperature and subsurface velocity to evaluate ice-sheet model spin-up and inversions.

Abstract

Ice streams are bounded by abrupt transitions in speed called shear margins. Some shear margins are fixed by subglacial topography, but others are thought to be self-organizing, evolving by thermal feedbacks to ice viscosity and basal drag which govern the stress balance of ice sheets. Resistive stresses (and properties governing shear-margin formation) manifest non-uniquely at the surface, motivating the use of subsurface observations to constrain modeled ice streams. In this study, we use radar data to evaluate three 3D thermomechanical models of the Northeast Greenland Ice Stream (NEGIS), focusing on the model reproductions of ice temperature (the primary control on viscosity) and subsurface velocity. Data/model agreement indicates elevated temperatures in the NEGIS margins, with depth-averaged temperatures between 2°C and 5°C warmer in the southeast margin, driven by vertical heat transport rather than shear heating. This work highlights complexity in ice velocity across stagnant/streaming transitions.

Plain Language Summary

Ice-sheet models used to project future sea-level rise are calibrated using modern observations of ice flow at the ice-sheet surface. However, the subsurface ice and rock properties that ultimately control the patterns of ice flow in Greenland cannot be uniquely determined using observations of the surface alone. In this study, we use the structural and electromagnetic characteristics of the Greenland Ice Sheet (determined from ice-penetrating radar data) to evaluate the subsurface performance of three different ice-flow models of the Northeast Greenland Ice Stream. We show that fast flow in Northeast Greenland is, in part, controlled by softer, warmer ice, and that correctly modeling heat transport at the boundaries of ice streams is critical for realistic projections of their future behavior. Ultimately, we provide insight into a sensitive region of Greenland together with a new approach to model evaluation, with the goal of reducing the range of plausible models projecting the future of the Greenland and Antarctic Ice Sheets.

1 Introduction

Predicting the future of Earth's ice sheets requires models that can first reproduce modern ice-sheet behavior. To do this, models rely on observations of ice-sheet surface velocity to infer the ice viscosity and substrate properties, which control the spatial pattern of ice flow (Joughin et al., 2004; MacAyeal, 1992; Morlighem et al., 2010). However, surface observations provide insufficient information to uniquely infer both ice viscosity and basal shear stress without additional constraints (Arthern & Gudmundsson, 2010). Models with equally good fits to surface observations can have different internal stress configurations, and therefore produce different projections of the ice-sheet response to climate forcing (Goelzer et al., 2018). Thus, there is need for new observational methods capable of inferring ice temperature, a critical influence on ice viscosity, and a necessary measurement for separating the englacial and basal stresses of ice streams.

1.1 Inferring Temperature and Velocity from Radar

Radar reflectivity and englacial layering have been the primary observations used to understand subsurface properties across shear margins. Reflectivity analysis has been focused on the bed, interpreting contrasts in reflection strength as wet to dry transitions across shear margins in Antarctica (Bentley et al., 1998; J. A. MacGregor et al., 2013; Raymond et al., 2006) and

Greenland (Christianson et al., 2014; Vallelonga et al., 2014). Disruptions in internal layering have been used to infer past margin position (Catania et al., 2006; Keisling et al., 2014). But, as new methods emerge in radioglaciology, radar data have the potential to provide more quantitative insight into temperature and heat transport, thought to govern shear margin behavior.

Radio waves are sensitive to elevated ice temperature, as the electrical conductivity of ice increases exponentially to the melting point (MacGregor et al., 2007). Power is lost to conduction as radio waves propagate through the ice, resulting in lower amplitude signals in warm or impurity rich areas. Thus, radio echo sounding data contains information about ice temperature and chemistry (Bogorodsky et al., 1985; Dowdeswell & Evans, 2004) as well as the electrical properties of subsurface reflectors (with variations typically attributed to subglacial water content or interface roughness). Substantial work has been done to disentangle attenuation signals from reflectivity without using an ice-sheet model (K Matsuoka et al., 2012; Schroeder et al., 2016), but available algorithms cannot provide robust attenuation estimates in the presence of temperature and reflector heterogeneity over small spatial scales. Thus, radioglaciologists have used ice sheet models to directly estimate attenuation effects (Matsuoka et al., 2012) and remove attenuation signals from radar data for more robust reflector interpretation (Chu et al., 2018).

In this study, we take a different approach. We use the spatial correlation between measured reflection strength and modeled temperature to validate the subsurface performance of ice sheet moels. This is possible because radar data contain independent information about both the thermal characteristics of ice (through measured reflection power) and the velocity structure (through englacial layer shapes, e.g. Hindmarsh et al., 2006; Holschuh et al., 2017; Leysinger Vieli et al., 2007). Discrepancies between modeled and inferred temperature are driven primarily by errors in the transport and production of heat in the subsurface, both a product of subsurface ice velocity. Thus, radar data have the potential to both identify errors in modeled temperature and isolate the processes responsible for the mismatch. We test this here using data from the shear margins of the Northeast Greenland Ice Stream (NEGIS), where temperature heterogeneity may be a controlling factor in shear localization.

1.2 Shear-margin mechanics in ice-flow models

Much of our understanding of thermally controlled ice-stream shear margins comes from a mix of 1D analysis (Meyer & Minchew, 2018; Perol & Rice, 2015) and 2D, flow-orthogonal thermomechanical modeling. Diagnostic modeling efforts first highlighted the role of frictional heat production in margin weakening (Jacobson & Raymond, 1998), predicting enhanced shear localization relative to isothermal ice when thermal softening is included in model physics. Model sophistication has increased dramatically since then, with modern models capable of simulating margin evolution, including the dynamic effects of melt-water production and subglacial hydrology (Elsworth & Suckale, 2016; Meyer et al., 2018; Perol et al., 2015; Suckale et al., 2014). However, to maintain numerical efficiency at very high resolution, 2D models use simplified ice dynamics, assuming the along-stream velocity evolves according to a reduced form of the momentum equations (excluding longitudinal stresses). Boundary-layer treatments of shear margins address this by solving the 3D Stokes equations, reproducing the heat production and advective cooling underpinning margin migration (Haseloff et al., 2015; Schoof, 2012); however, these models use a fixed value of ice viscosity, and rely on an idealized geometry (assuming no vertical velocities in basal ice resting on a flat bed) to simplify the calculation.

Comparing results of simplified models to realistic ice-stream systems requires evaluating the impact of their simplifying assumptions. This is especially important for margins with ice that flows across the stagnant/streaming boundary, as previous studies show that reproducing the depth-velocity structure across abrupt boundary-condition transitions requires the inclusion of longitudinal stresses (Hindmarsh et al., 2006). In this study, we use 3D, full-Stokes diagnostic modeling (Gagliardini et al., 2013) to simulate the complex heat generation and transport across a realistic ice-stream margin.

We focus on the incipient shear margins of NEGIS (Fig. 1), where shear localization manifests amid diffuse flow acceleration. As with other shear margins, the position of the incipient margin may be imposed by the underlying geology (Anandakrishnan et al., 1998; J. A. MacGregor et al., 2013). But it is also possible that these margins are self-organizational, forming by a thermal perturbation reinforced by temperature feedbacks within the ice (Jacobson & Raymond, 1998; Suckale et al., 2014), fabric development (Minchew et al., 2018), and/or subglacial hydrologic organization (Elsworth & Suckale, 2016; Kyrke-Smith et al., 2015; Perol et al., 2015; Perol & Rice, 2015). By diagnosing the thermal structure in the incipient margin, we can evaluate whether geologic controls are required to explain the velocity pattern, or if the margin is collocated with a thermal anomaly that will influence its future evolution.

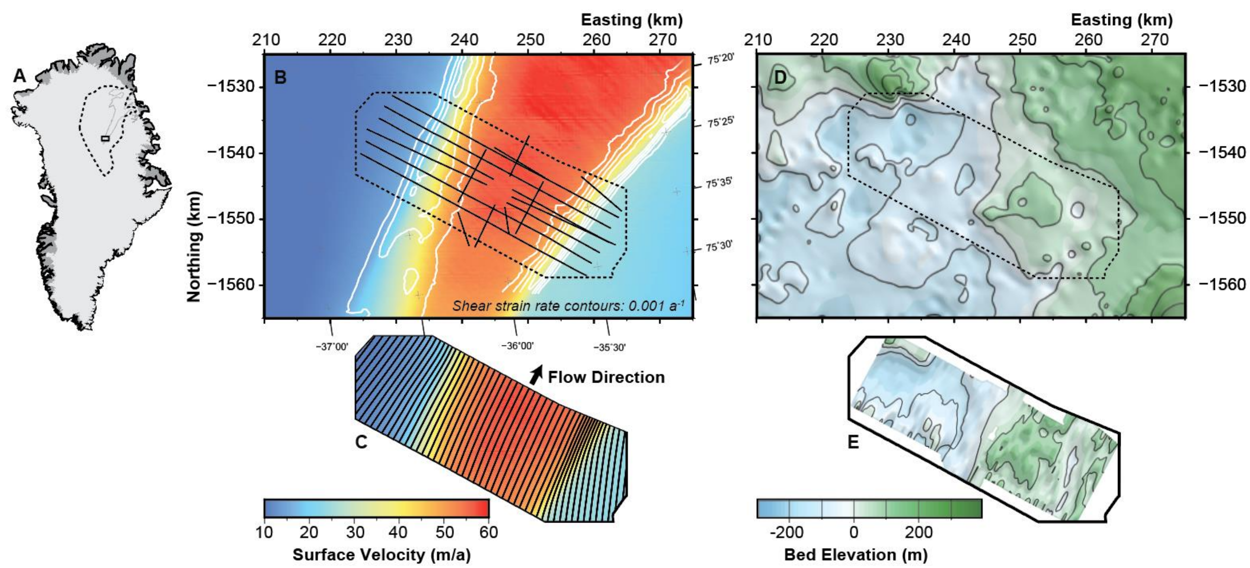

Figure. 1 – Regional context for the Northeast Greenland Ice Stream (A), presenting both the ice surface velocity (B,C – [I. Joughin et al., 2016]) and bed topography (D – [Bamber et al., 2013], E – inverse distance weighted interpolation of radar data presented in this study). The full catchment and high-resolution model domain are provided as dotted lines in (A) and (B,D), respectively, with radar profile locations plotted as black lines in (B). Ice-flow streamlines are provided in (C), highlighting cross-marginal flow in the SE margin of NEGIS. (Map projection - EPSG:3413)

2 Methods

2.1 Modeling the Northeast Greenland Ice Stream

We use a 3D, full-Stokes, thermomechanical model, implemented in Elmer/Ice (Gagliardini et al., 2013; Zwinger et al., 2007) to reproduce the dynamics of the NEGIS margins. This is done in two stages. The first stage, a full-catchment model (9 vertical layers, 500m-5000m mesh refined around the area of interest), was used to generate temperature and velocity boundary conditions for the second stage, a higher-resolution (~100m mesh) model, designed to span the 2012 radar survey across the incipient NEGIS margins. The model experiment set-up, boundary conditions, and implementation are described in the Supplementary Material.

In modeling this system, we found that the observed surface velocity, accumulation rate, and ice thickness are difficult to rectify with one another assuming steady-state mass balance. This mismatch likely arises from a combination of data limitations (e.g., spatially incomplete ice thickness measurements or poorly reconstructed accumulation rates) and missing physics in the model (e.g., ice fabric evolution), and is a common challenge in ice-sheet modeling. Models typically address this mismatch in one of three ways: (1) the ice surface is allowed to relax in accordance with ice velocities (as in Larour et al. (2014) and Brondex at al. (2019)), resulting in a model with matching surface velocities but erroneous ice thickness, (2) the surface velocities are scaled to bring the system into balance given the measured geometry and accumulation rate, resulting in a disagreement between observed and modeled horizontal flow speeds (as in Zwinger et al. (2007)), or (3) the ice thickness and horizontal velocities are imposed, and the vertical velocities are assumed to provide balance, allowing disagreement with accumulation rates at the surface (as in Pattyn (2010)).

Without an a priori justification for one method over the others, we produced three realizations of our model domain following published procedures. This resulted in two equilibrium reproductions (following methods 1 and 2) and one disequilibrium reproduction of NEGIS (following method 3). We differentiate these models in text and figures according to their agreement with ice thickness (H), horizontal velocities at the surface (u,v, for polar-stereographic coordinate axes x and y), and vertical velocities at the surface (w, with positive values upward). Ultimately, our goal is to use radar data to evaluate the performance of these three models and use observations together with the best-fit model to better understand the dynamics of the NEGIS shear margins.

2.2 Radar Processing and Interpretation

The radar data used in this study were collected in summer 2012 and were first published as part of Christianson et al. (2014), who detail the initial processing (including geolocation, bandpass filtering, correction for antenna spacing, travel time correction for firn density, interpolation to standard trace spacing, along-track migration, and geometric spreading correction to return amplitude). For this study, the effects of geometric spreading and refractive focusing through the firn column were removed following the methods of Holschuh et al. (2016), and the remaining variations in the bed reflection power are attributed to spatial variability in ice conductivity or substrate permittivity. Physical interpretation of measured reflection power requires disambiguating the effects of these two properties.

2.3 Conductivity Modeling

Converting modeled ice temperature to radar-wave attenuation requires conductivity modeling. Conductivity in ice is treated as a thermally activated process, with models requiring impurity concentrations, activation energies, and temperatures (MacGregor et al., 2007). Using average impurity concentrations during the Holocene and Glacial period as observed in the GRIP ice core (which has the most complete, local, soluble impurity record) (De Angelis et al., 1997), and the reflector known to separate these two periods in the radar data, we define a depth-impurity profile for each radar trace. This assumes constant impurity concentration within a given layer package, requiring that layer thickness differences primarily reflect differential divergence and not a spatially variable snow accumulation rate upstream (which could drive impurity dilution). Using the modeled temperature profiles, we calculate the associated conductivity and depth-averaged attenuation rates using parameters found in the literature (Gudmandsen, 1971; MacGregor et al., 2015; MacGregor et al., 2007; Wolff et al., 1997), and present a model/data inter-comparison for the best-fit model (see Supplementary Fig. 2,3 for model selection process).

2.3 Model/Data Correlation

To evaluate consistency between model temperature and radar reflectivity, we compute local linear fits between modeled and observed reflection strength. Regression statistics (specifically R^2 values) for local fits indicate the spatial agreement between the modeled temperature field and the pattern of observed reflection strength. Fit coefficients for the local linear regressions indicate the agreement in magnitude of the temperature anomalies – a fit coefficient of 1 indicates the modeled and observed power losses match perfectly, while coefficients between 0 and 1 (i.e., observed power losses divided by modeled power losses < 1) indicate modeled conductivity (and therefore modeled temperature) is likely too high. Overall NEGIS model performance is presented as an addition R^2 statistic, computed using the aggregated residual sum of squares from the local fits.

3 Results

3.1 Depth-averaged temperature fields

The depth averaged temperature fields for our three model realizations are presented in Figure 2. Figure 2.A presents the results for a model of NEGIS with a relaxed surface, in which ice thickness is 30m thicker than observed in the shear margins. Figure 2.B presents a model with horizontal flow speeds reduced to bring the system into mass balance, with streaming flow speeds 10-15 m/a slower than observed. Figure 2.C presents the model that matches the observed geometry and horizontal flow speeds, but has a mean error of ~2 m/a for vertical velocities at the surface.

Each of our three model realizations produced a different depth-averaged temperature field, with the most dramatic differences between our equilibrium and disequilibrium cases (Fig. 2A,B vs. 2C). The model with a relaxed surface resulted in the highest average temperature over the full domain (Fig. 2A). This model showed slightly elevated temperatures in the SE margin (~2-3°C), with no clear temperature anomaly in the NW margin. The steady state model with lower streaming flow speeds (Fig. 2B) has a clear thermal signature in both margins (~2°C), but generally colder ice within the ice stream. In contrast, the disequilibrium model has much stronger thermal anomalies in the margins than the steady-state runs (SE, ~5-6°C and NW, ~4-5°C). While the equilibrium models predict stronger thermal anomalies on the upstream end of the domain, the disequilibrium model has no along-flow trend.

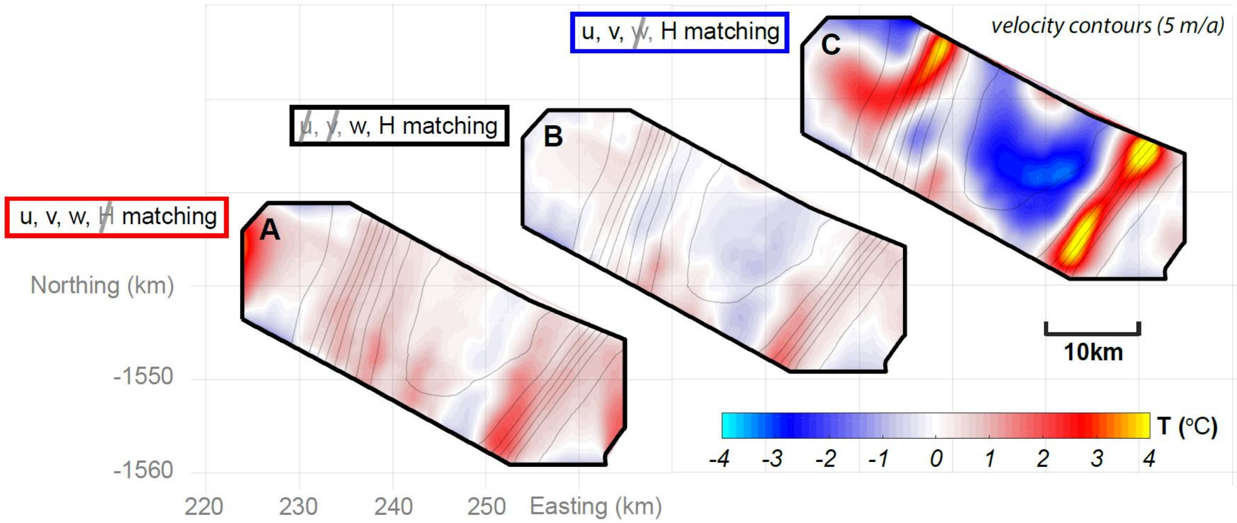

Figure 2. – Depth-averaged temperature anomalies (relative to -14°C) for models using three different boundary forcings: (A) steady-state, relaxed surface conditions, (B) steady-state, forced geometry but reduced velocity conditions, and (C) surface elevation and horizontal velocity matching, but surface-flux imbalance conditions. Surface velocity contours (5 m/a) are presented to highlight the position of the ice-stream shear margins.

3.2 Radar Isochrons, Subsurface Velocity, and Heat Advection

Variability in shear strain rates between models is small (~ 0.001 a^{-1}), and thus differences in heat production by viscous dissipation are negligible. Differences in depth-averaged temperature are largely the result of heat transport through the domain. Radar imaged isochrons provide context for heat transport, as their relative heights in the ice column reflect differential transport through time. There is always ambiguity when interpreting englacial structures – assuming steady-state, structures form in place, but with boundary condition changes through time, it is possible to form a fold elsewhere and advect to its observed location in the modern ice sheet. Because the observed folds are collocated with the modern shear margins along the full trunk of NEGIS, we assume they formed in place.

There are several characteristics of the imaged isochrons and surface velocity field that can inform our understanding of the system:

1. Distinct fold structures were imaged in the shear margins in all flow-orthogonal lines (Fig. 3A). Isochrons are at their shallowest (highest) point in the ice column within the shear margins.

2. Layer deflections are largest for the deepest imaged layers, decreasing in amplitude

toward the surface.

3. Ice passes through the SE margin (from where isochrons are deep, to where they are shallow, back to deep) within our model domain, while ice flow is sub-parallel to the NW margin fold (see Fig. 1C, Supplementary Fig. 4).

These conditions constrain fold generation mechanism in several ways. Ice passing through the SE shear margin must be driven upward within our model domain by substantial vertical velocities at depth. These velocities could be imparted by direct forcing at the bed in the form of basal freeze-on (Fig 3C.ii), or could be the result of convergence and layer thickening in the deepest parts of the ice, increasing velocities and layer deflections up column to the point where layers are imaged (Fig 3C.i). Ice in the NW is also experiencing differential vertical transport in and outside the margin, but because ice does not pass through the margin here, particles within a given layer do not have a shared transport history and the fold structure cannot be definitively attributed to processes within our model domain. The NW folds could have formed upstream, or by local cross-flow convergence. Decreasing fold amplitudes higher in the ice column indicate divergence and layer thinning, reducing the magnitude of vertical velocities imposed by the deep ice. As ice passes into streaming flow from the shear margins and layers drop, deep layers must thin (or there must be compensating basal melt at depth within streaming flow), driving negative vertical velocities.

Using the 3D velocity field for each of our three models, we synthesize layers assuming they enter the domain at constant depth. The resulting synthetic isochrons highlight perturbations to layer depth that occur within the model domain, where local structures such as the SE shear-margin folds must have formed. We produce these for all three model realizations, extract the layer geometries at the radar observation sites, and plot the results against the modeled depth-temperature profiles (Fig. 3D-F).

Vertical advection of ice dominates the modeled thermal structure in all three cases, with high temperatures shallower in the ice column where upwarping layers are predicted. The steady-state models resulted in flat or slightly downwarped layers in the margins, different from both the disequilibrium model and the observations, which have fold amplitudes of ~500 m in the central portion of the ice column. These form in the model by deep along- and across-flow convergence without requiring basal freeze-on, thought to be limited at NEGIS (Dow et al., 2018).

There is unresolved disagreement between the modeled and observed isochrons in the upper portion of the ice column, where fold amplitudes are damped in the data. This could be explained by compensating divergence in the upper half of the ice column not captured in our model (but seen in models of flow over bed friction anomalies in Holschuh et al., (2017) and Whillans and Johnsen (1983)).

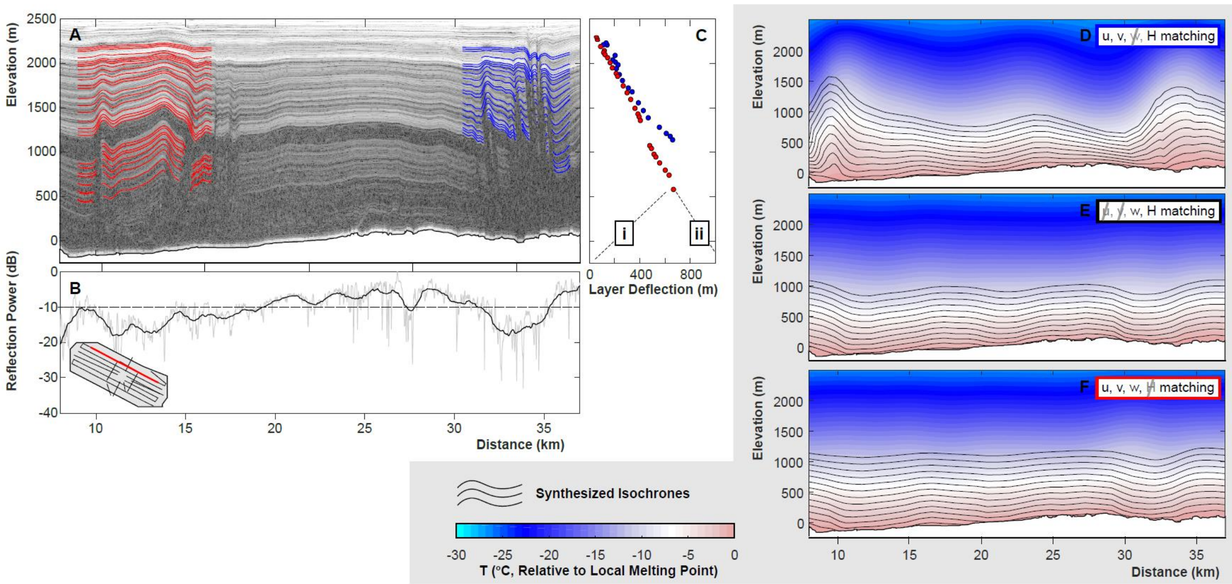

Figure 3. – Characteristic radargram (A) collected at the downstream end of the model domain, with the associated bed reflection strength corrected for spherical spreading and refractive focusing through the firn (B). Layers imaged in the shear margins show increasing deflection with depth (C), down to where they can no longer be imaged. Near the bed, layers must either be bed conformal, with increasing upward deflection due to layer thickening by flow convergence (i), or non-conformal with vertical deflections equal to the thickness of basal freeze-on at the bed (ii). For the same transect, synthetic isochrons and modeled temperature are presented (D-F).

3.3 Radar Reflection Strength and Modeled Temperature

Within the shear margins, weaker bed returns are collocated with upwarped englacial layers (Fig 3.B, Fig 4.A). In general, reflection power / temperature agreement is better for the SE margin across all models, and better for the disequilibrium model than the equilibrium models. Local fits between expected and observed power losses (Fig 4.B) show the equilibrium models systematically underestimating power losses in the margins (fit coefficients > 1), with little ability to explain trends in reflection power ($R^2 < 0.5$). The disequilibrium model typically overestimates the magnitude of the temperature anomaly (fit coefficients between 0 and 1), but has substantial ability to explain the spatial pattern of power losses. This is highlighted in the overall model fits (Fig 4.C) with better performance by the disequilibrium model across all regions. Surprisingly, the western edge of the NW margin shows a negative correlation between expected and observed power loss for all models, indicating that either (a) the temperature models have warm ice where it should be cold, or (b, more likely) that the modeled spatial pattern of warm ice, which matches the spatial pattern of bright reflection, is an indicator of basal water outside the NW margin.

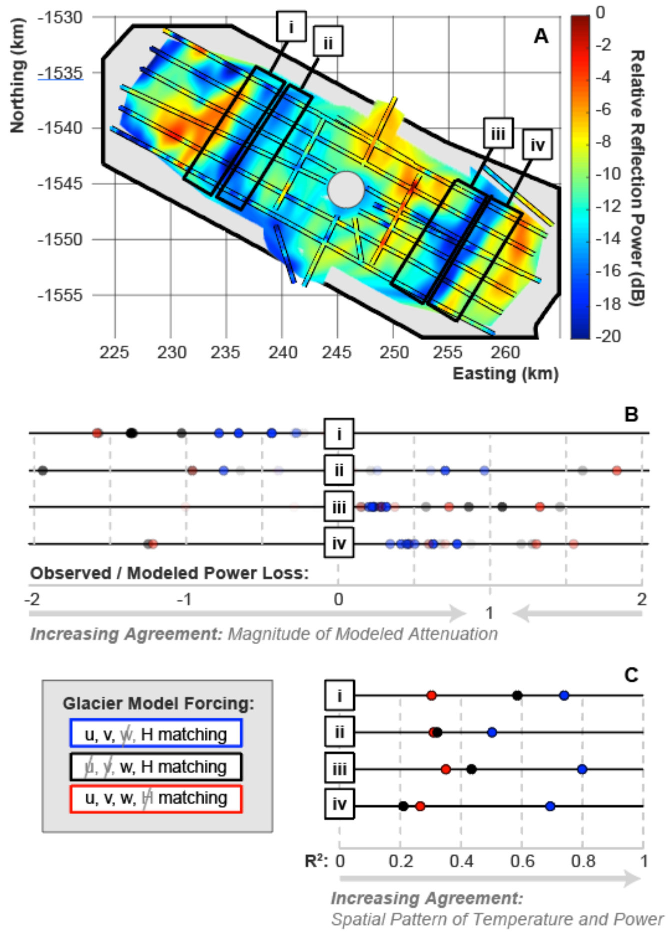

Figure 4. – Plot of the bed reflection power (A). The correlation between modeled and observed bed power (colored by model boundary forcing) is computed for each radar line as they cross in-to (i, iv) and out-of (ii, iii) the shear margins. The coefficient relating modeled and observed power loss for each local fit is presented in (B) (with opacity representing the R^2 significance of each local regression). The overall R^2 for subdomains i-iv, indicative of the total agreement between model and observation, is presented in (C), highlighting the superior performance of our disequilibrium model across all four regions of interest.

4. Discussion

4.1 Evidence for elevated temperature at NEGIS

NEGIS is defined by 400 km long shear margins, with no indication of topographic control for at least 200 km in its upstream reaches (Fig. 1D,E). Shear localization (as opposed to diffuse acceleration as seen in most ice-stream catchments) implies that there is an abrupt change in strength across the stagnant-streaming transition, but it is otherwise unknown if this is a change in rock properties, effective stress at the bed, ice viscosity, or a combination of all three. The spatial pattern of bed reflection power matches the disequilibrium modeled temperature field well in the SE margin, suggesting significant vertical advection (and the warm ice) is present at

NEGIS and weakens the margins.

4.2 The role of advection in the thermal balance of shear margins

Heat retention in shear margins is ultimately an advection-diffusion problem, illustrated conceptually by the following equation:

$$\rho c_p u \frac{\partial T}{\partial x} + \rho c_p v \frac{\partial T}{\partial y} + \rho c_p w \frac{\partial T}{\partial z} = K \frac{\partial^2 T}{\partial z^2} + \sigma_{ij}\epsilon_{ij} \quad (1)$$

Comparing the product of modeled temperature gradients $\left(\frac{\partial T}{\partial x}, \frac{\partial T}{\partial y}, \frac{\partial T}{\partial z}\right)$ and their corresponding velocities (u,v,w, respectively) with the total rate of strain heating (defined as the product of the Cauchy stress tensor $\boldsymbol{\sigma_{ij}}$ and strain rate tensor $\boldsymbol{\epsilon_{ij}}$), it is possible to determine the dominant processes acting to modify temperature within our model domain. We do this using published values for the presented physical constants (density - $\boldsymbol{\rho}$: 917 kg m^{-3}, specific heat capacity - $\boldsymbol{c_p}$: 2050 J kg^{-1} K^{-1}), and thermal conductivity - $\boldsymbol{K}$: 2.1 W m^{-1} K^{-1}). Given maximum shear strain rates in our domain of 0.005 a^{-1}, and modeled vertical and horizontal temperature gradients of ~0.01 K/m and ~0.001 K/m respectively, the advective terms of the thermal balance have comparable influence to shear heating when the vertical velocity is ~0.02 m/a or cross-marginal velocities exceed ~0.2 m/a.

Cross-marginal velocities rise well above this threshold at NEGIS, with values of ~4 m/a for the western margin and ~10 m/a in the eastern margin (see Supplementary Fig. 5). Thus, we would expect advective cooling to dominate over shear heating. In addition, simple treatments of vertical velocity (assuming it is negative and less than or equal to the accumulation rate of ~0.1 m/a at our site) imply accumulation driven cooling would overcome any strain warming.

However, subglacial topography and flow convergence drive vertical velocities deep in the ice column across all 3 models, resulting in values of $\boldsymbol{w}$ well above the significance threshold. Maximum vertical velocities in our equilibrium runs fall between 0.25 and 0.5 m/a, and exceeds 1 m/a in our disequilibrium run, expected at NEGIS given substantial layer slopes in the shear margins (Holschuh et al., 2017). With high vertical temperature gradients, even small differences in vertical velocity become important. Ultimately, velocities deep in the ice column dominate the thermal structure and attenuation signal at NEGIS (as variations in the thickness of high temperature ice have a disproportionate effect on depth averaged conductivity). Isochron geometries (which follow isotherms in our model results – Fig. 3.D-F) may provide a direct observational method for estimating relative temperature across slow flowing regions, as relative layer depths reflect differences in net-vertical advection.

5 Conclusions

We present here the first radar-validated, 3D thermomechanical model of an ice-stream shear margin and show that fast flow at NEGIS is facilitated. in part by thermally weakened ice. Models that fail to capture the deep vertical velocity structure will underestimate thermal weakening in the ice, compensate by underestimating the strength of the ice bed, and ultimately fail to reproduce the system dynamics.

Structural and intensity information from radar data act as independent checks on modeled ice velocity and temperature, and highlight a previously undescribed role for vertical advection in shear margins, which dominates here over heat production and shear-margin cooling effects from cross-marginal flow. We show that the velocity structure, temperature field, and resulting strength of the ice for this ice-stream system differ significantly from idealized characteristics inferred from surface observations alone. Flow convergence is likely to drive thermal margin development at other incipient shear margins, as vertical advection creates the initial thermal weakness that is reinforced by subsequent shear localization.

Acknowledgments, Samples, and Data

N. Holschuh developed the study and performed the radar analysis and radar-model intercomparison. D. Lilien implemented the model. Christianson collected and processed the radar data and contributed to the interpretation. All authors participated in writing. Radar data and model output are accessible through the University of Washington's ResearchWorks Archive (doi available after acceptance). NASA grant no. NNX16AM01G and NSF grant no. 1643353 supported N. Holschuh and K. Christianson. NASA grant no. NNX15AN53H supported D. Lilien.

References

Anandakrishnan, S., Blankenship, D. D., Alley, R. B., & Stoffa, P. L. (1998). Influence of subglacial geology on the position of a West Antarctic ice stream from seismic observations. *Nature*, *394*(6688), 62–65. https://doi.org/10.1038/27889

De Angelis, M., Steffensen, J. P., Legrand, M., Clausen, H., & Hammer, C. (1997). Primary aerosol (sea salt and soil dust) deposited in Greenland ice during the last climatic cycle: Comparison with east Antarctic records. *Journal of Geophysical Research: Oceans*, *102*(C12), 26681–26898. https://doi.org/10.1029/97JC01298

Arthern, R. J., & Gudmundsson, G. H. (2010). Initialization of ice-sheet forecasts viewed as an inverse Robin problem. *Journal of Glaciology*, *56*(197), 527–533. https://doi.org/10.3189/002214310792447699

Bamber, J. L., Griggs, J. A., Hurkmans, R. T. W. L., Dowdeswell, J. A., Gogineni, S. P., Howat, I., et al. (2013). A new bed elevation dataset for Greenland. *The Cryosphere*, *7*(2), 499–510. https://doi.org/10.5194/tc-7-499-2013

Bentley, C. R., Lord, N., & Liu, C. (1998). Radar reflections reveal a wet bed beneath stagnant Ice Stream C and a frozen bed beneath ridge BC, West Antarctica. *Journal of Glaciology*, *44*(146), 149–156. https://doi.org/10.1073/pnas.1100349108

Bogorodsky, V., Bentley, C., & Gudmandsen, P. (1985). *Radioglaciology* (1st ed.). Dordrecht, Holland: D. Reidel Publishing Co.

Brondex, J., Gillet-Chaulet, F., & Gagliardini, O. (2019). Sensitivity of centennial mass loss projections of the Amundsen basin to the friction law. *The Cryosphere*, *13*(1), 177–195. https://doi.org/10.5194/tc-13-177-2019

Catania, G. A., Scambos, T. A., Conway, H., & Raymond, C. F. (2006). Sequential stagnation of Kamb Ice Stream, West Antarctica. *Geophysical Research Letters*, *33*(14), 2–5. https://doi.org/10.1029/2006GL026430

Christianson, K., Peters, L. E., Alley, R. B., Anandakrishnan, S., Jacobel, R. W., Riverman, K. L., et al. (2014). Dilatant till facilitates ice-stream flow in northeast Greenland. *Earth and Planetary Science Letters*, *401*, 57–69. https://doi.org/10.1016/j.epsl.2014.05.060

Chu, W., Schroeder, D. M., Seroussi, H. S., Creyts, T. T., & Bell, R. E. (2018). Complex basal thermal transition near the onset of Petermann Glacier, Greenland. *Journal of Geophysical Research: Earth Surface*, 1–11. https://doi.org/10.1029/2017JF004561

Dow, C. F., Karlsson, N. B., & Werder, M. A. (2018). Limited impact of subglacial supercooling freeze-on for Greenland Ice Sheet stratigraphy. *Geophysical Research Letters*. https://doi.org/10.1002/2017GL076251

Dowdeswell, J. A., & Evans, S. (2004). Investigations of the form and flow of ice sheets and glaciers using radio-echo sounding. *Reports on Progress in Physics*, *67*(10), 1821–1861.

https://doi.org/10.1088/0034-4885/67/10/R03

Elsworth, C. W., & Suckale, J. (2016). Subglacial drainage may induce rapid ice flow rearrangement in West Antarctica. *Geophysical Research Letters*, *43*, 11697–11707. https://doi.org/10.1002/2016GL070430

Gagliardini, O., Zwinger, T., Gillet-Chaulet, F., Durand, G., Favier, L., De Fleurian, B., et al. (2013). Capabilities and performance of Elmer/Ice, a new-generation ice sheet model. *Geoscientific Model Development*, *6*(4), 1299–1318. https://doi.org/10.5194/gmd-6-1299-2013

Goelzer, H., Nowicki, S., Edwards, T., Beckley, M., Abe-Ouchi, A., Aschwanden, A., et al. (2018). Design and results of the ice sheet model initialisation experiments initMIP-Greenland: an ISMIP6 intercomparison. *The Cryosphere*, *12*, 1433–1460.

Gudmandsen, P. (1971). Electromagnetic probing of ice. In J. Wait (Ed.), *Electromagnetic Probing in Geophysics* (pp. 321–348). Boulder, CO: Golem Press.

Haseloff, M., Schoof, C., & Gagliardini, O. (2015). A boundary layer model for ice stream margins. *Journal of Fluid Mechanics*, *781*, 353–387. https://doi.org/10.1017/jfm.2015.503

Hindmarsh, R. C. A., Leysinger Vieli, G. J. M. C., Raymond, M. J., & Gudmundsson, G. H. (2006). Draping or overriding: The effect of horizontal stress gradients on internal layer architecture in ice sheets. *Journal of Geophysical Research: Earth Surface*, *111*(2). https://doi.org/10.1029/2005JF000309

Holschuh, N., Christianson, K., Anandakrishnan, S., Alley, R. B., & Jacobel, R. W. (2016). Constraining attenuation uncertainty in common midpoint radar surveys of ice sheets. *Journal of Geophysical Research: Earth Surface*, *121*(10), 1876–1890. https://doi.org/10.1002/2016JF003942

Holschuh, N., Parizek, B. R., Alley, R. B., & Anandakrishnan, S. (2017). Decoding ice sheet behavior using englacial layer slopes. *Geophysical Research Letters*, *44*(11), 5561–5570. https://doi.org/10.1002/2017GL073417

Jacobson, H. P., & Raymond, C. E. (1998). Thermal effects on the location of ice stream margins. *Journal of Geophysical Research*, *103*(B6), 12,111-12,22.

Joughin, I., Smith, B., Howat, I., & Scambos, T. (n.d.). MEaSUREs Greenland Ice Sheet Velocity Map from InSAR Data, Version 2. Boulder, Colorado USA: NASA National Snow and Ice Data Center Distributed Active Archive Center. https://doi.org/http://dx.doi.org/10.5067/OC7B04ZM9G6Q

Joughin, I., MacAyeal, D. R., & Tulaczyk, S. (2004). Basal shear stress of the Ross ice streams from control method inversions. *Journal of Geophysical Research B: Solid Earth*, *109*(9), 1–20. https://doi.org/10.1029/2003JB002960

Keisling, B. A., Christianson, K., Alley, R. B., Peters, L. E., Christian, J. E. M., Anandakrishnan, S., et al. (2014). Basal conditions and ice dynamics inferred from radar-derived internal stratigraphy of the northeast Greenland ice stream. *Annals of Glaciology*, *55*(67), 127–137. https://doi.org/10.3189/2014AoG67A090

Kyrke-Smith, T. M., Katz, R. F., & Fowler, A. C. (2015). Subglacial hydrology as a control on emergence, scale, and spacing of ice streams. *Journal of Geophysical Research: Earth Surface*, *120*, 1501–1514.

Larour, E., Utke, J., Csatho, B., Schenk, A., Seroussi, H., Morlighem, M., et al. (2014). Inferred basal friction and surface mass balance of North-East Greenland Ice Stream using data assimilation of ICESat-1 surface altimetry and ISSM. *The Cryosphere*, *8*(1), 2331–2373. https://doi.org/10.5194/tcd-8-2331-2014

Leysinger Vieli, G. J.-M. C., Hindmarsh, R. C. a, & Siegert, M. J. (2007). Three-dimensional flow influences on radar layer stratigraphy. *Annals of Glaciology*, 22–28.

MacAyeal, D. R. (1992). The basal stress distribution of Ice Stream E, Antarctica, inferred by control methods. *Journal of Geophysical Research*, *97*(B1), 595. https://doi.org/10.1029/91JB02454

MacGregor, J., Li, J., Paden, J. D., Catania, G. A., Clow, G. D., Fahnestock, M. A., et al. (2015). Radar attenuation and temperature within the Greenland Ice Sheet. *Journal of Geophysical Research: Earth Surface*, (120), 983–1008. https://doi.org/10.1002/2014JF003418.Received

MacGregor, J. A., Winebrenner, D. P., Conway, H. B., Matsuoka, K., Mayewski, P. A., & Clow, G. D. (2007). Modeling englacial radar attenuation at Siple Dome, West Antarctica, using ice chemistry and temperature data. *Journal of Geophysical Research*, *112*(F3), 1–14. https://doi.org/10.1029/2006JF000717

MacGregor, J. A., Catania, G. A., Conway, H., Schroeder, D. M., Joughin, I., Young, D. A., et al. (2013). Weak bed control of the eastern shear margin of Thwaites Glacier, West Antarctica. *Journal of Glaciology*, *59*(217), 900–912. https://doi.org/10.3189/2013JoG13J050

Matsuoka, K., MacGregor, J. A., & Pattyn, F. (2012). Predicting radar attenuation within the Antarctic ice sheet. *Earth and Planetary Science Letters*, *359–360*, 173–183. https://doi.org/10.1016/j.epsl.2012.10.018

Matsuoka, K., Pattyn, F., Callens, D., & Conway, H. (2012). Radar characterization of the basal interface across the grounding zone of an ice-rise promontory in East Antarctica. *Annals of Glaciology*, *53*(60), 29–34. https://doi.org/10.3189/2012AoG60A106

Meyer, C. R., & Minchew, B. M. (2018). Temperate ice in the shear margins of the Antarctic Ice Sheet: Controlling processes and preliminary locations. *Earth and Planetary Science Letters*, *498*, 17–26. https://doi.org/10.1016/j.epsl.2018.06.028

Meyer, C. R., Yehya, A., Minchew, B., & Rice, J. R. (2018). A Model for the Downstream Evolution of Temperate Ice and Subglacial Hydrology Along Ice Stream Shear Margins.

Journal of Geophysical Research: Earth Surface, *123*(8), 1682–1698. https://doi.org/10.1029/2018JF004669

Minchew, B. M., Meyer, C. R., Robel, A. A., Gudmundsson, G. H., & Simons, M. (2018). Processes controlling the downstream evolution of ice rheology in glacier shear margins: case study on Rutford Ice Strea , West Antarctica. *Journal of Glaciology*, 1–12. https://doi.org/10.1017/jog.2018.47

Morlighem, M., Rignot, E., Seroussi, H., Larour, E., Ben Dhia, H., & Aubry, D. (2010). Spatial patterns of basal drag inferred using control methods from a full-Stokes and simpler models for Pine Island Glacier, West Antarctica. *Geophysical Research Letters*, *37*(14), 1–6. https://doi.org/10.1029/2010GL043853

Pattyn, F. (2010). Antarctic subglacial conditions inferred from a hybrid ice sheet/ice stream model. *Earth and Planetary Science Letters*, *295*(3–4), 451–461. https://doi.org/10.1016/j.epsl.2010.04.025

Perol, T., & Rice, J. R. (2015). Shear heating and weakening of the margins of West Antarctic ice streams. *Geophysical Research Letters*, *42*(9), 3406–3413. https://doi.org/10.1002/2015GL063638

Perol, T., Rice, J. R., Platt, J. D., & Suckale, J. (2015). Subglacial hydrology and ice stream margin locations. *Journal of Geophysical Research F: Earth Surface*, *120*(7), 1352–1368. https://doi.org/10.1002/2015JF003542

Raymond, C. F., Catania, G. A., Nereson, N., & Van Der Veen, C. J. (2006). Bed radar reflectivity across the north margin of Whillans Ice Stream, West Antarctica, and implication for margin processes. *Journal of Glaciology*, *52*(176), 3–10. https://doi.org/10.3189/172756506781828890

Schoof, C. (2012). Thermally driven migration of ice-stream shear margins. *Journal of Fluid Mechanics*, *712*, 552–578. https://doi.org/10.1017/jfm.2012.438

Schroeder, D. M., Seroussi, H., Chu, W., & Young, D. A. (2016). Adaptively constraining radar attenuation and temperature across the Thwaites Glacier catchment using bed echoes. *Journal of Glaciology*, *62*(236), 1075–1082. https://doi.org/10.1017/jog.2016.100

Suckale, J., Platt, J. D., Perol, T., & Rice, J. R. (2014). Deformation-induced melting in the margins of the West-Antarctic ice streams. *Journal of Geophysical Research: Earth Surface*, *119*, 1004–1025. https://doi.org/10.1002/2013JF003008

Vallelonga, P., Christianson, K., Alley, R. B., Anandakrishnan, S., Christian, J. E. M., Dahl-Jensen, D., et al. (2014). Initial results from geophysical surveys and shallow coring of the Northeast Greenland Ice Stream (NEGIS). *Cryosphere*, *8*(4), 1275–1287. https://doi.org/10.5194/tc-8-1275-2014

Whillans, I. M., & Johnsen, S. J. (1983). Longitudinal variations in glacial flow: theory and test using data from the Byrd Station strain network, Antarctica. *Journal of Glaciology*, *29*(101), 78–97.

Wolff, E. W., Miners, W. D., Moore, J. C., & Paren, J. G. (1997). Factors Controlling the Electrical Conductivity of Ice from the Polar RegionsA Summary. *The Journal of Physical Chemistry B*, *101*(32), 6090–6094. https://doi.org/10.1021/jp9631543

Zwinger, T., Greve, R., Gagliardini, O., Shiraiwa, T., & Lyly, M. (2007). A full Stokes-flow thermo-mechanical model for firn and ice applied to the Gorshkov crater glacier, Kamchatka. *Annals of Glaciology*, *45*, 29–37. https://doi.org/10.3189/172756407782282543

Figure 1.

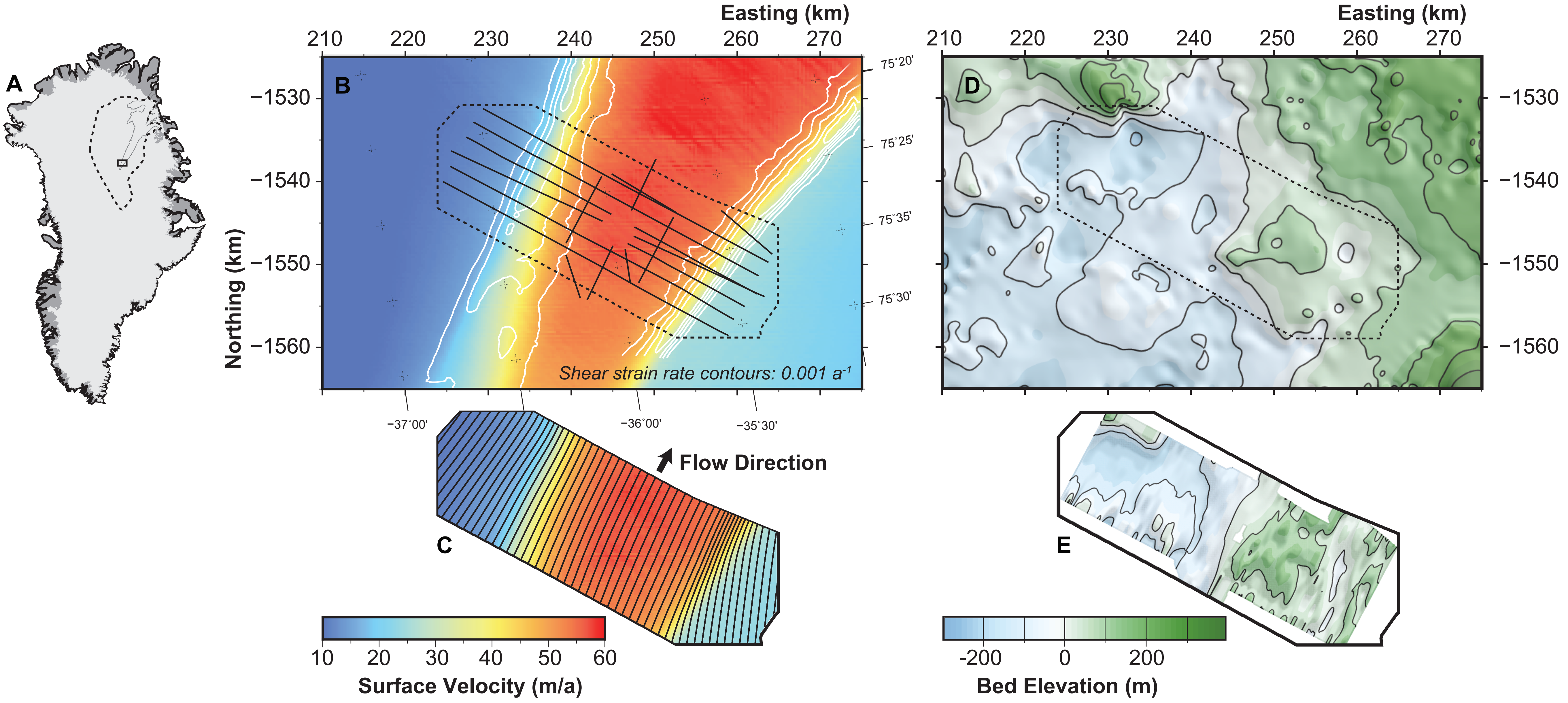

A
B
C
D
E
Easting (km)
210
220
230
240
250
260
270
Northing (km)
−1530
−1540
−1550
−1560
75°20'
75°25'
75°35'
75°30'
−37°00'
−36°00'
−35°30'
Shear strain rate contours: 0.001 a⁻¹
Flow Direction
10
20
30
40
50
60
Surface Velocity (m/a)
−200
0
200
Bed Elevation (m)

Figure 2.

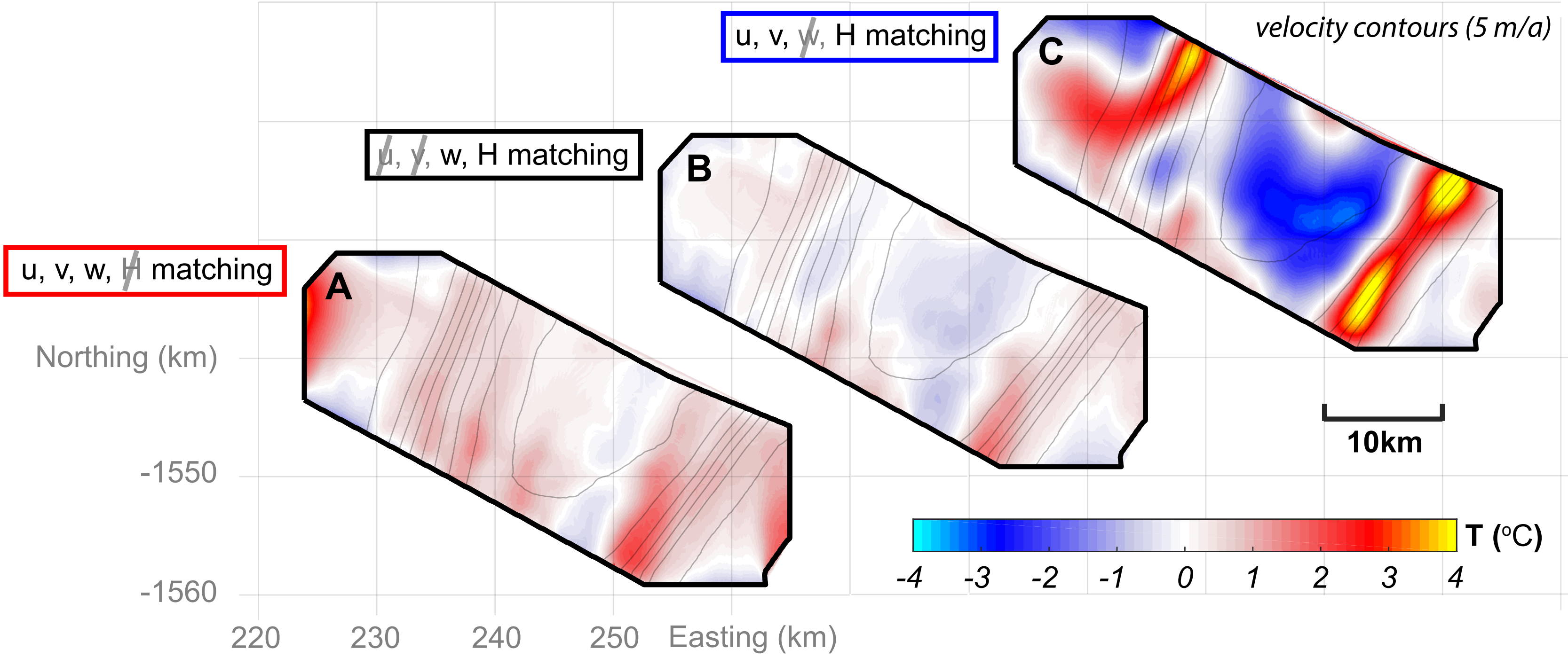

u, v, ~~w~~, H matching
~~u~~, ~~v~~, w, H matching
u, v, w, ~~H~~ matching
A
B
C
velocity contours (5 m/a)
10km
T (°C)
-4
-3
-2
-1
0
1
2
3
4
Northing (km)
-1550
-1560
220
230
240
250
Easting (km)

Figure 3.

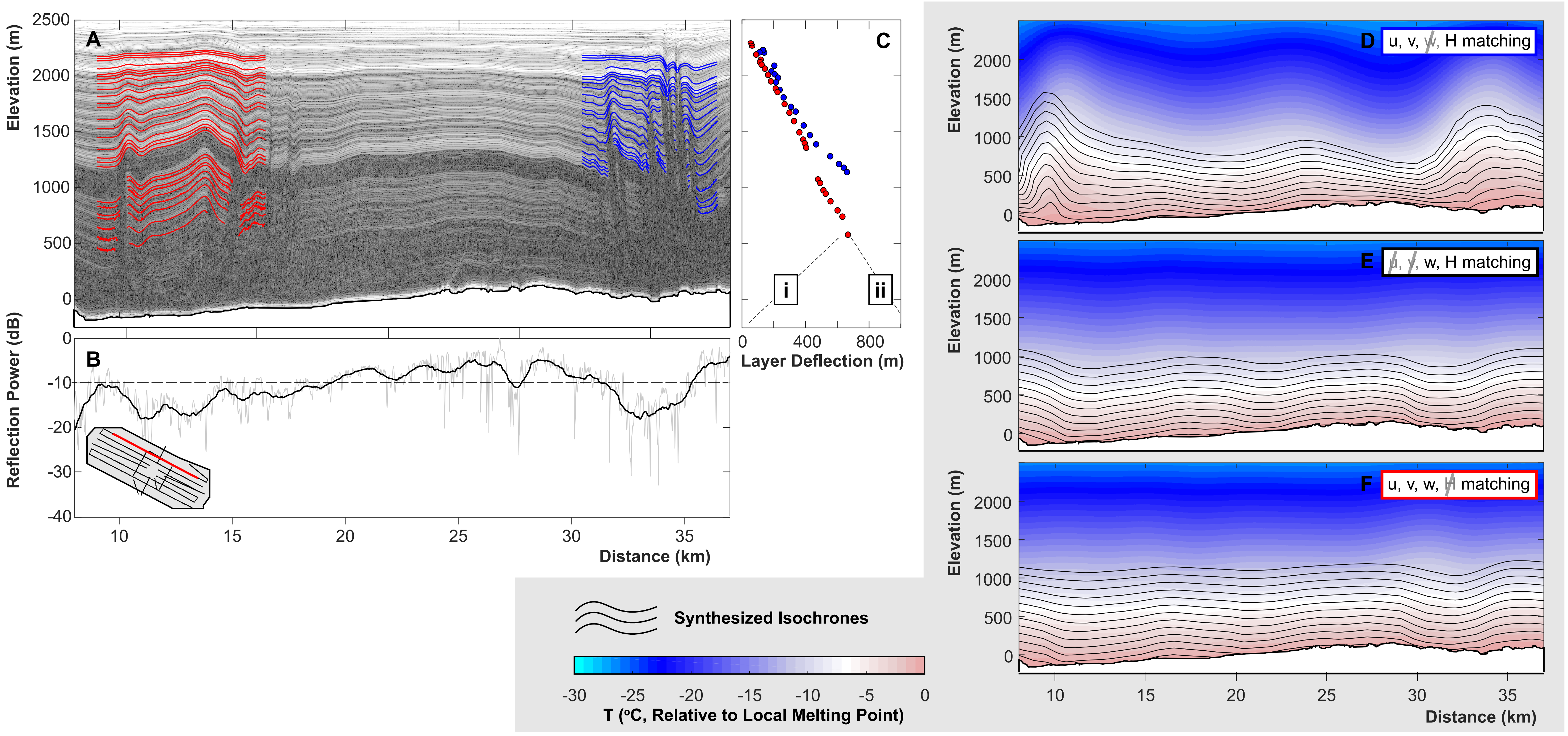

A
B
C
D
E
F
Elevation (m)
Reflection Power (dB)
Layer Deflection (m)
Distance (km)
i
ii
u, v, ~~w~~, H matching
~~u~~, ~~v~~, w, H matching
u, v, w, ~~H~~ matching
Synthesized Isochrones
T (ºC, Relative to Local Melting Point)

Figure 4.

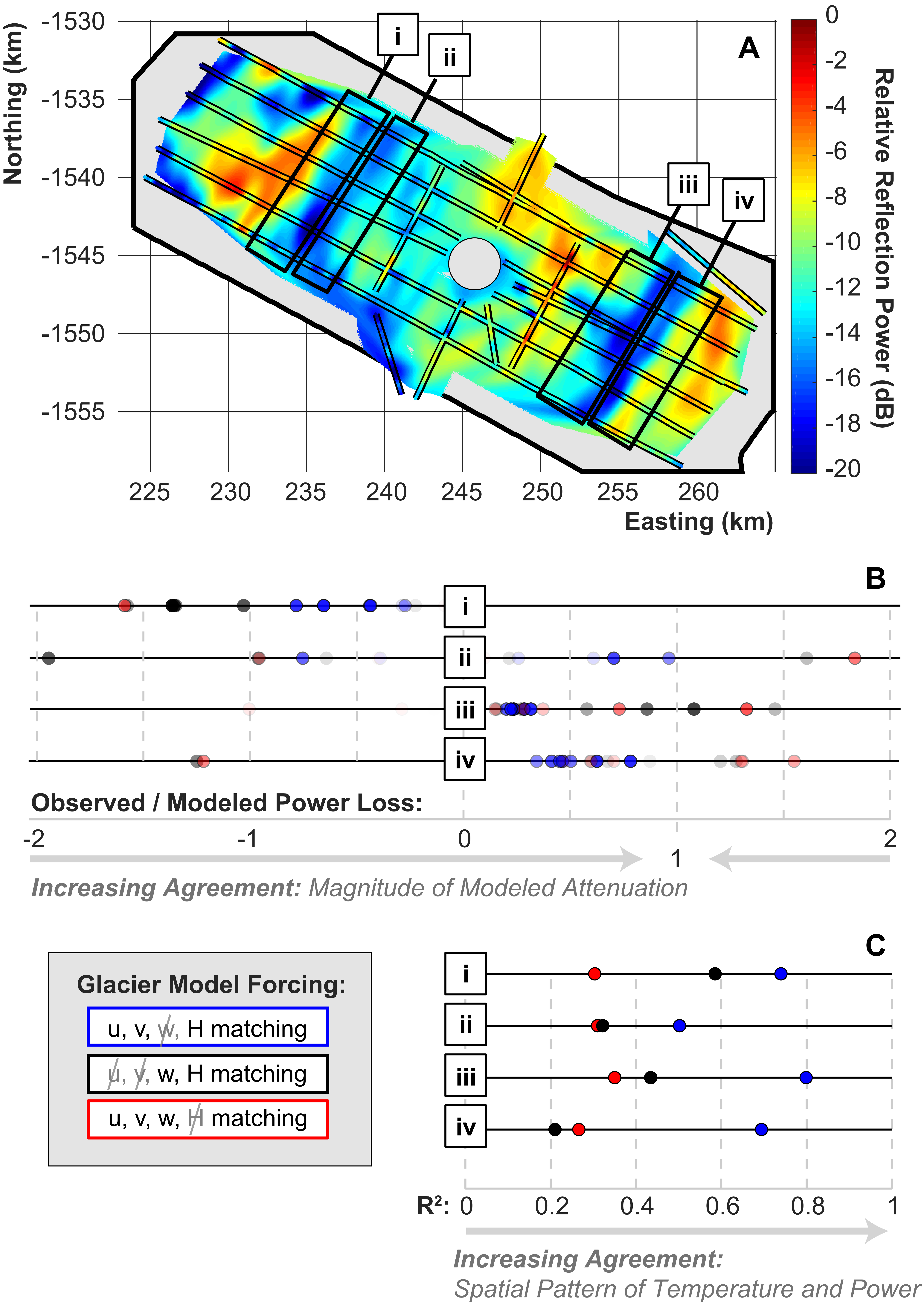

A
B
C
Northing (km)
Easting (km)
Relative Reflection Power (dB)
i
ii
iii
iv
Observed / Modeled Power Loss:
Increasing Agreement: Magnitude of Modeled Attenuation
R²:
Increasing Agreement:
Spatial Pattern of Temperature and Power
Glacier Model Forcing:
u, v, ~~w~~, H matching
~~u~~, ~~v~~, w, H matching
u, v, w, ~~H~~ matching